INSTITUTE OF PHYSICS PUBLISHING PLASMA SOURCES SCIENCE AND TECHNOLOGY

Plasma Sources Sci. Technol. **10** (2001) 226–235 www.iop.org/Journals/ps PII: S0963-0252(01)22648-6

Time-resolved measurements of the electron energy distribution function in a helicon plasma

David D Blackwell[1] **and Francis F Chen**

Electrical Engineering Department, University of California, Los Angeles, CA 90095-1594, USA

Received 7 July 2000, in final form 21 February 2001

Abstract

An energy analyser with the capability of making time-resolved measurements of the instantaneous electron current in a radiofrequency (RF) plasma has been designed and constructed. This current is then reconstructed into the instantaneous I–V characteristic at various phases of the RF cycle. Results are shown for a helicon wave discharge under various conditions. From the first derivative of the I–V characteristic, it is observed that there is an absence of high-energy electrons characteristic of strong Landau damping, suggesting that some other mechanism is responsible for the discharge's high ionization efficiency.

1. Introduction

One of the prevailing explanations for the helicon discharge's high ionization efficiency is that of collisionless heating in the form of Landau damping [1]. This mechanism can produce a population of fast electrons in the electron energy distribution function (EEDF), dramatically affecting the ionization rate. The most direct evidence of this would be found by measuring the distribution function itself. In theory [2], Landau damping would cause a flattening of this function in the vicinity of $v = v_\phi$, the wave's phase velocity. The effect on the EEDF and on a Langmuir probe characteristic is shown in figure 1, where for simplicity's sake we have modelled the altered Maxwellian distribution as a function of the form [3]

$$f(u) \propto \exp\left(-\int_0^u \frac{t\,\mathrm{d}t}{t+g(t)}\right) \tag{1}$$

where u is the velocity normalized to the thermal velocity, and $g(t)$ is defined as

$$g(t) = \begin{cases} \infty & u_1 < u < u_2 \\ 0 & \text{otherwise.} \end{cases} \tag{2}$$

Over the past decade, experiments based on probes were performed in which the results seemed to confirm the Landau damping hypothesis. In 1991, Zhu and Boswell [4] reported a double-humped distribution function which disappeared 1 μs after the discharge was started. In a later experiment, Loewenhardt *et al* [5] reported a similar observation in a toroidal plasma, with the double hump remaining for the duration of the plasma (20 ms). Also observed was the fact that the wave field structure within the torus had a correlation with the energy of the electron tail. In another experiment performed by Mieno *et al* [6], measurements of the EEDF taken with a velocity analyser demonstrated that the energy of the tail could be controlled by changing the RF frequency. Molvik *et al* [7, 8] recently used an electron energy analyser to detect a 20 eV pulsed electron beam which was consistent with the measured phase velocity of their helicon wave. Most recently, Chen and Hershkowitz [9] measured multiple electron beams in a helicon plasma which qualitatively agreed with the measured spectrum of phase velocities.

The one common element that these experiments share is that all of the important data were obtained with electrostatic probes or similar diagnostics. Unfortunately, measurements made with such tools suffer from complications arising from RF pick-up. This is especially true for the helicon discharge, which may have large RF fluctuations in the electron temperature T_e, the density n, and the space potential V_s. As pointed out by Hershkowitz [10], the averaging of these changes can lead to a distorted characteristic (figure 2), which looks very much like the expected result of Landau damping. In the aforementioned experiments, these problems with the diagnostics were only lightly addressed. In particular, although the design of RF-compensated Langmuir probes is well known, the gridded energy analysers used were not RF

[1] Current address: US Naval Research Laboratory, Plasma Physics Division, Washington, DC 20375, USA.

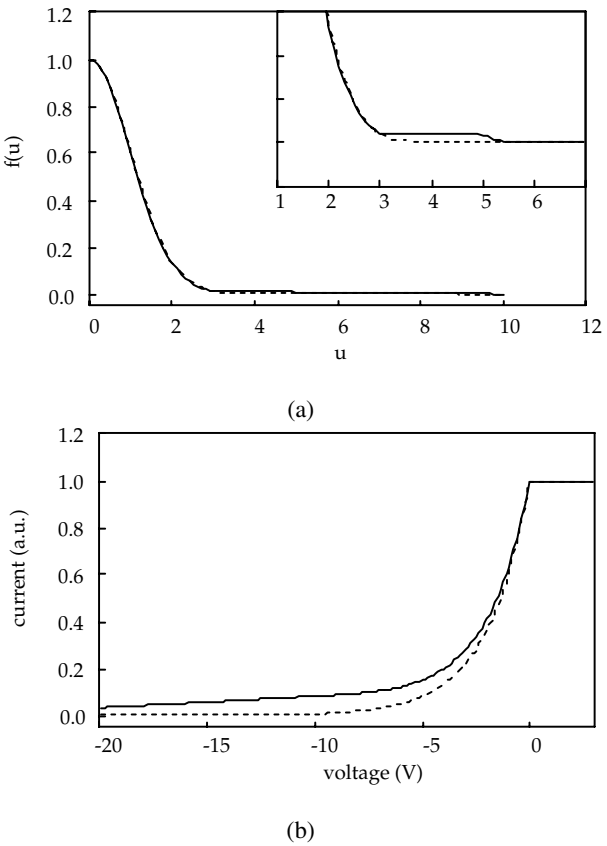

Figure 1. Computed curves showing an example of the effect of Landau damping on (a) the distribution function and (b) the corresponding probe characteristic. The dashed lines show the curves from an ordinary Maxwellian. A small distortion (2%) around $3 < u < 5$ of the distribution function ((a) inset) leads to a significant change in the measured current.

compensated and were subject to the same nonlinear averaging as uncompensated probes.

Our first attempt at a solution was the design of a narrow-band, high-impedance probe [11]. The high impedance circuit acts as a voltage divider between the fluctuating sheath voltage and the rest of the probe circuit, as shown in figure 3(a). The probe will follow the voltage oscillations by satisfying the condition

$$\frac{Z_{sh}}{Z_{sh}+Z_c}V_{plasma} \ll KT_e \tag{3}$$

with Z_{sh} the sheath impedance, Z_c the probe circuit impedance, and V_{plasma} the RF fluctuating part of the plasma (space) potential. As seen in figure 3(b), this compensated probe gives very different results from an ordinary probe. On cursory examination, the normal probe characteristic would seem to indicate a large population of fast electrons.

Although this probe was a great improvement, it still addressed only one problem, that of fluctuating potential. Any fluctuations in the distribution function itself would still be averaged or masked altogether. This became a greater concern after the experiment of Ellingboe *et al* [12], in which a strong RF modulation of an Ar^+ emission line was detected. The intensity peak was observed to propagate along the magnetic field with a velocity close to the helicon wave phase velocity. The light excitation was attributed to a population of energetic electrons, moving through the plasma, which are accelerated during a specific phase of the wave travelling at its phase velocity. This proposed mechanism could be corroborated by measuring the instantaneous EEDF at specific phases in the RF cycle. It was to this end that we designed an energy analyser capable of such a measurement. In a previous paper [20], we presented an overview of the experimental results. This paper deals with more specifics of the analyser design, experimental technique, and data obtained.

2. Energy analyser design

In a plasma with time-varying EEDF and V_s, the instantaneous current to a flat surface biased at potential V with respect to V_s can be written as

$$i_{t=t_0} = eA\int_{-\infty}^{\infty}\int_{-\infty}^{\infty}\int_{\sqrt{-2eV_0/m}}^{\infty} v_\parallel f(v_\parallel, \boldsymbol{v}_\perp, t_0)\,\mathrm{d}v_\parallel\,\mathrm{d}\boldsymbol{v}_\perp + C_{sh}(V_0)\left.\frac{\mathrm{d}V}{\mathrm{d}t}\right|_{t=t_0} \tag{4}$$

where V_0 is the potential at time $t = t_0$, and $v_\parallel$, $\boldsymbol{v}_\perp$ are the parallel and perpendicular components of the velocity with respect to the surface normal. The second term in this expression is the capacitive current through the time-varying plasma sheath. The sheath capacitance can be derived by approximating an ion sheath thickness from the Child–Langmuir law; this is approximately [13]

$$C_{sh}(V) = en_eA_{sh}\frac{3}{4}\left(\frac{2}{eM}\right)^{1/4}\left(\frac{1}{9\pi j_i}\right)^{1/2}V^{-1/4} \tag{5}$$

with A_{sh} being the sheath area and j_i the ion flux through the sheath, which in general is also a function of potential. When a probe measurement is performed, there is no way to separate these two currents, which can be of comparable magnitude. Figure 4 compares this capacitive (displacement) current with the electron current in a Maxwellian plasma. The small currents from higher energy electrons are in some instances smaller than the capacitive current. It is therefore crucial to reduce this capacitive current to as small a value as possible; otherwise, it could be mistaken for current from hyperthermal electrons. If it were not for this capacitive current, the instantaneous EEDF could be obtained with an ordinary Langmuir probe. The key function of the energy analyser is to separate the electron current from this unwanted signal; in fact, this is the *only* way to do this with a probe-based diagnostic.

The principal difference between a gridded analyser and a Langmuir probe is that the surface which actually collects the electrons in an analyser has no plasma sheath around it. The sheath is instead formed around a discriminator grid set in front of a collector. Since there is no sheath, the capacitive current to the collector will be reduced to the capacitive current between itself and this grid.

These considerations affect the design in two essential ways. First, the grid spacing must be small enough to shield out any plasma from passing through it. This can be guaranteed by making $l < \lambda_D$, with l the grid spacing and λ_D the plasma Debye length. The grid for our analyser was made of 2000 lpi nickel mesh, which had a grid spacing of about 6 μm. With

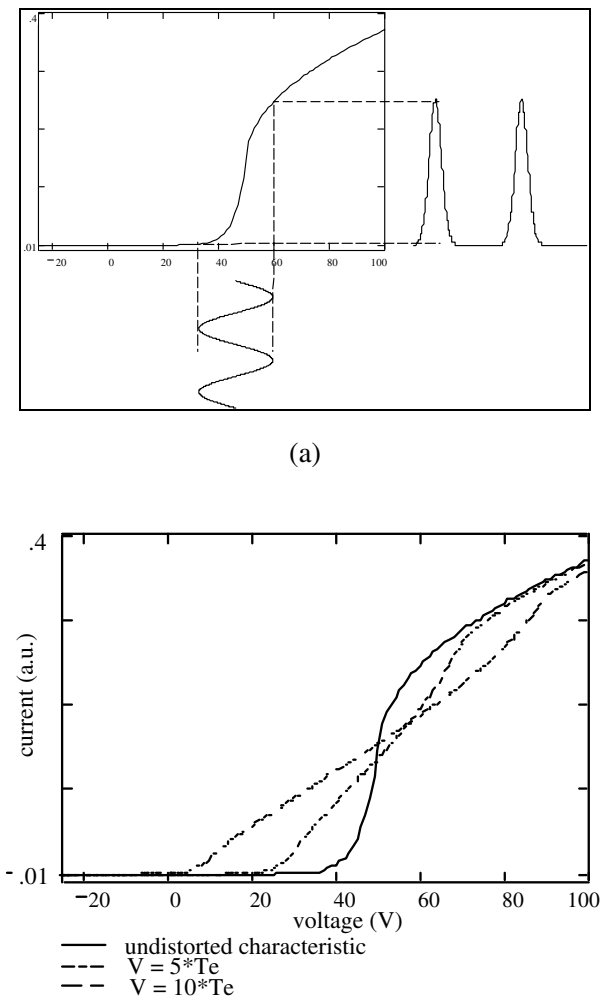

Figure 2. The mechanism and result of RF distortion: (a) illustrates how the swing in voltage maps out a current with a non-zero time average due to the nonlinearity of the probe characteristic; (b) shows numerically computed characteristics for different amplitudes of RF voltage at the probe, showing the severe distortion caused by the time-averaged currents collected at different voltages.

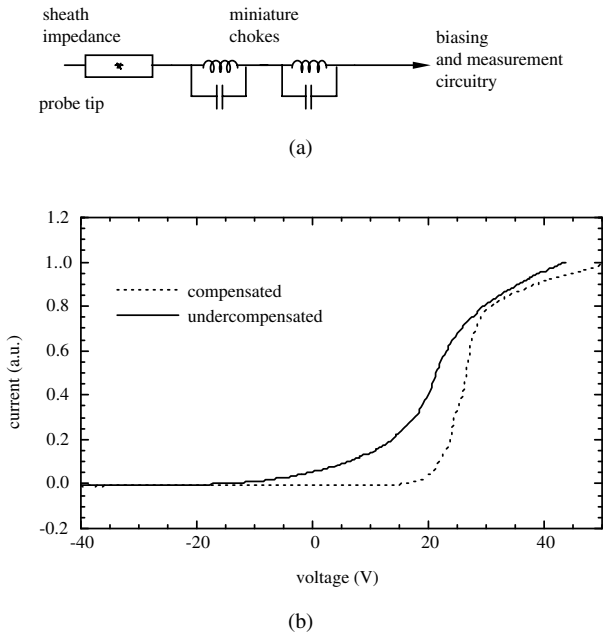

Figure 3. (a) A simplified circuit diagram of the compensated probe, and (b) its measured characteristic compared with an under-compensated probe. Both curves were recorded under the same plasma conditions. The full curve represents the poorly compensated probe characteristic, which on cursory inspection would seem to have a more energetic population of electrons. Even with filters installed, it does not satisfy equation (3), and thus suffers distortion due to the oscillating sheath potential.

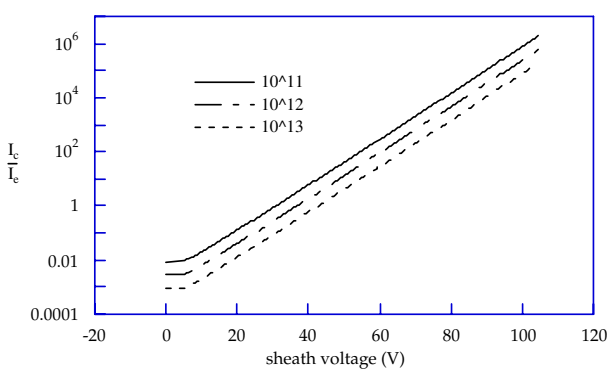

Figure 4. Computed plot of the ratio of capacitive current from equation (4) to electron current for three plasma densities in units of cm^{-3} for an electron temperature of 3 eV. The measurement of energetic electrons becomes increasingly more susceptible to error as the capacitive current from the oscillating sheath becomes comparable to the real electron current with increasing sheath voltage.

the highest density plasmas we could produce ($\sim 10^{13}$ cm^{-3}), this would be less than two Debye lengths at a temperature of 3 eV; under these conditions we could expect that, in the retardation region at least, the grid would sufficiently block any plasma from reaching the collector [21]. To test this, we biased the grid and the collector at opposite high potentials. This test was actually required to periodically check for damage to the extremely fragile nickel mesh. Second, the spacing between the grid and the collector must be less than any electron collision length to ensure that the electrons which pass through the grid reach the collector unimpeded, and that no ionizing collisions occur in the region between the two. This was a much easier condition to satisfy, since for our parameters all the collision lengths were a centimetre or more, while the spacing between the grid and the collector was only 2 mm. The physical layout of the analyser is shown in figure 5(a).

The fact that the analyser would be working in an RF environment and collecting high-frequency signals required additional modifications. The discriminator grid was shunted to the grounded stainless steel housing of the analyser with a 10 nF capacitor (C_x) to hold it at a fixed potential. This capacitor forms an impedance divider between the plasma and collector plate to suppress the capacitive current signal. This is effective for values of $C_x \gg C_p$, where C_p is the plasma sheath capacitance. This was satisfied for all experimental conditions. The collector and grid were wired to the biasing and measurement circuitry with 50 Ω micro-coax, and the signal from the collector was terminated in a matched load. We found from past experience that this type of transmission

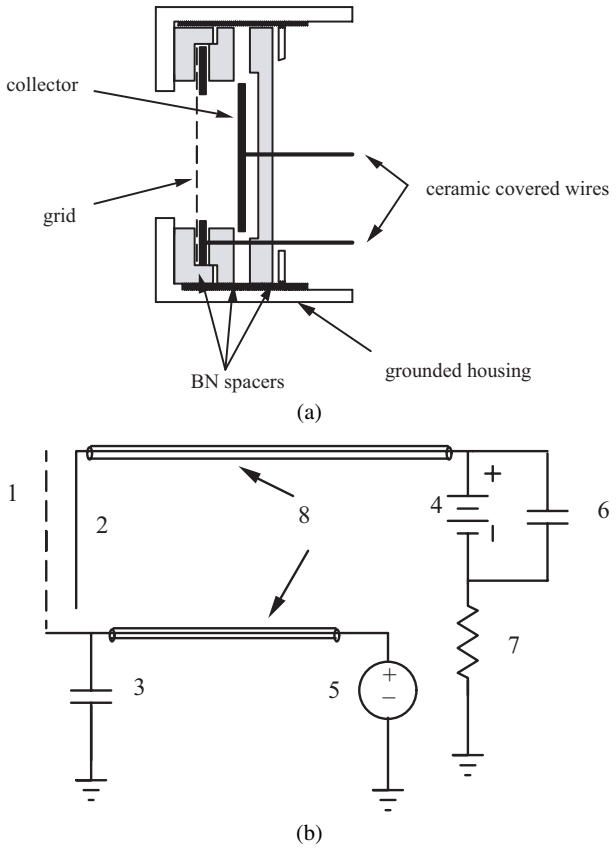

Figure 5. (a) Physical layout of the analyser, shown at approximately twice actual size. (b) Electric circuit equivalent. The grid (1) is biased with variable dc power supply (5) and shunted directly to the stainless steel housing through the capacitor C_x (3). The collector set 2 mm behind the grid is biased with a +300 V battery (4), while another shunting capacitor (6) offers a low impedance path for the high frequency signals. To insure good shielding against unwanted stray signals and good frequency response, the collector and grid are connected to their respective biasing circuits through copper-jacketed 50 Ω micro-coax, with the collector current being measured with a 50 Ω oscilloscope termination.

and measurement set-up gave the best frequency response. All shields were grounded at a single point at the output of the matching circuit. Figure 5(b) shows the electrical schematic of the analyser.

3. Experimental procedure and calibrations

The experimental apparatus used is a 10 cm diameter helicon plasma source described in detail elsewhere [14]. It consists of a 10 cm diameter cylindrical glass chamber 100 cm long surrounded by eight large magnetic field coils, which can supply a field of 350–1000 G. The RF antenna strapped to the outside of the chamber can be placed at various positions along its length. The energy analyser was oriented with the plane of the grid perpendicular to the magnetic field in all cases. A drawing of the experimental set-up is shown in figure 6.

To test the accuracy of the analyser, an electron gun was built. The gun (figure 7(a)) consisted of a heated tantalum filament wound in a 3 cm diameter spiral and negatively biased to act as a cathode. A tungsten screen was positioned 3 mm in front of it to act as an anode. Figure 7(b) shows the electron emittance curve of the gun with the anode grounded. The beam current roughly follows the Child–Langmuir law, indicating space-charge-limited emission. The anode was then capacitively coupled to a function generator so that the intensity and energy of the electron beam could be modulated. This apparatus was mounted at one end of the discharge chamber, with the analyser facing it from the opposite end through a vacuum feedthrough. In the analyser, the discriminator grid voltage was set with a variable power supply, while the collector was biased with a +300 V battery to collect electrons and repel ions.

Figure 8 shows a representative dc vacuum characteristic of the beam as measured by the analyser. With the capacitive current eliminated, the first derivative of this current in the electron retardation region is related to the EEDF by the equation

$$f(v_\parallel) \propto \left[\frac{\mathrm{d}i}{\mathrm{d}V}\right]_{eV=1/2mv_\parallel^2} \tag{6}$$

with $f(v_\parallel)$ defined as

$$f(v_\parallel) \equiv \int_{-\infty}^{\infty}\int_{-\infty}^{\infty} f(v_\parallel, \boldsymbol{v}_\perp)\,\mathrm{d}\boldsymbol{v}_\perp. \tag{7}$$

Thus, for an isotropic plasma this derivative represents the actual distribution of electron energy, as shown in figure 8. When this beam is fired into argon gas, it creates a plasma with a distribution function similar to those previously observed for the helicon discharge [4, 5, 9]. Figures 9 and 10 show the evolution of this distribution function over pressure and distance from the gun. This gave a first-hand reference for the characteristic features we would later be looking for in the helicon plasma.

With the analyser working satisfactorily on our simple dc plasma, the next task was to evaluate its performance in a time-varying situation. A 13.56 MHz modulation signal was applied to the anode, which simulated the effect of a rapidly changing distribution function. As the anode voltage is varied, the energy and number of electrons emitted from the gun changes. When the beam is fired into argon, the resulting plasma also has its potential modulated. We can then simulate a plasma with a changing distribution function and a changing potential. As these parameters change, the collector current will be a nonlinear mapping of the anode voltage. Figure 11(a) shows the instantaneous electron current in a weakly ionized gun-produced plasma with the anode modulated. By varying the analyser's grid voltage, we can record this signal at a specific phase of the RF to reconstruct the I–V characteristic at a specific time; or, equivalently, for a specific distribution function and plasma potential. Essentially, we would be taking a 'snapshot' of the rapidly changing characteristic. This is a logical, more detailed extension of the measurements reported by Molvik *et al* [7, 8], where the instantaneous current signal at one fixed grid voltage was measured.

A test of this reconstruction method was performed by first measuring the characteristic at two dc operating points, set by adjusting the filament bias. The bias was then set half way between these two voltages, and a 13.56 MHz sinusoidal modulation signal was fed to the anode. The peak-to-peak amplitude of the anode signal was adjusted to match the

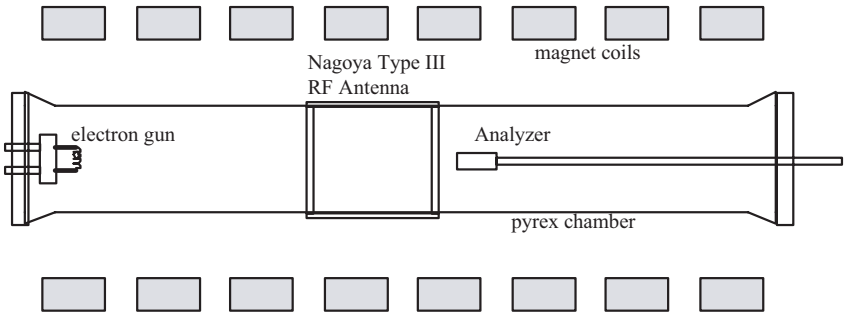

Figure 6. Diagram of the experimental apparatus. For RF plasma measurements the analyser is positioned on-axis, 20 cm from the nearest end of the antenna.

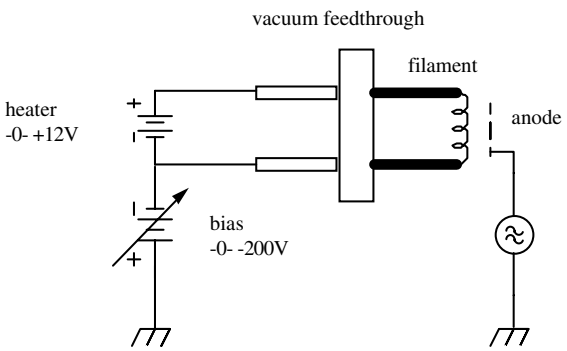

(a)

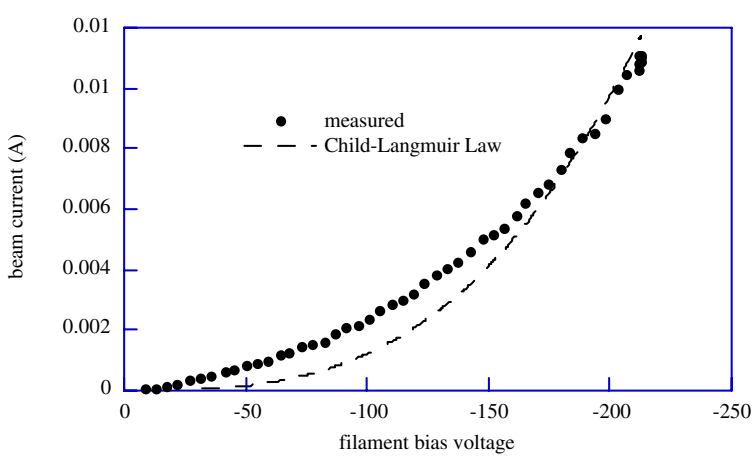

(b)

Figure 7. (a) Diagram of the electron gun with modulated anode. (b) The vacuum emission characteristic of the electron gun (●) compared with the space charge limit (- - - -).

voltage difference between the two dc operating points. By recording the current signal to the collector at the phases of the anode signal corresponding to these extreme points and varying the grid voltage, we had snapshots that we could compare with the dc characteristics. Figure 11(b) shows that the curves reconstructed from the modulated beam agree well with the curves measured under dc conditions. The same procedure was duplicated using a moderate density plasma ($n \sim 10^{11}$ cm^{-3}), the results of which are shown in figure 12. Again the reconstructed curves showed excellent agreement with the dc curves. For comparative purposes, measurements of the time-averaged characteristic were taken using an RF-compensated Langmuir probe, as described earlier. As could be expected, this probe characteristic fell between the dc curves. The electron temperature measured was slightly higher (40%). Figure 13 shows that, for a plasma with a pronounced high-energy tail, the RF modulation causes these fast electrons to be preferentially suppressed in the probe

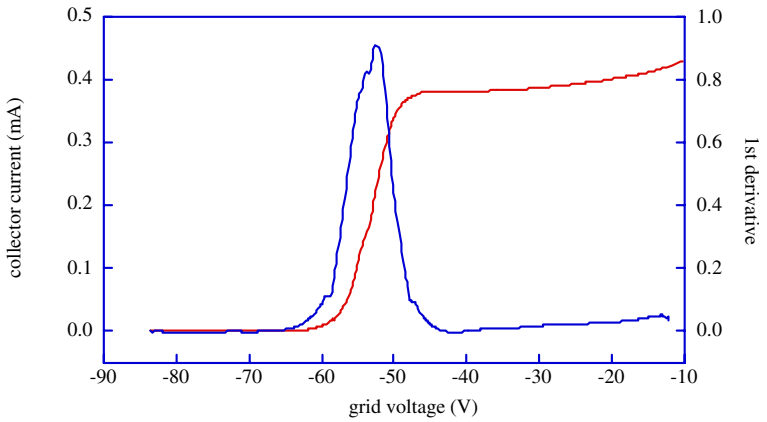

Figure 8. Electron analyser measurement of an electron beam in vacuum. The monotonic curve is collector current versus discriminator voltage (left scale); the peaked curve is its normalized first derivative (right scale). The gun is 50 cm from the analyser and has a filament bias of −52 V, and the dc magnetic field is 350 G.

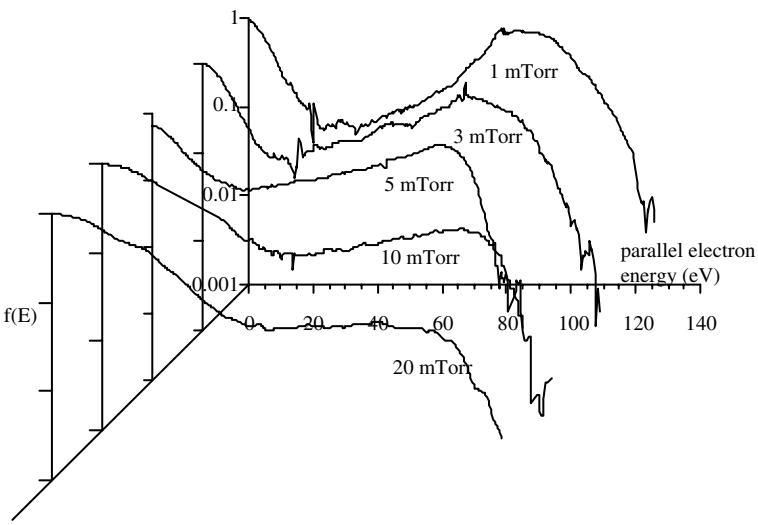

Figure 9. Evolution of the beam–plasma distribution function in a magnetic field with increasing neutral gas pressure at a distance of 5 cm from the electron gun. The gun is dc biased at −80 V with the anode removed. The beam electrons, characterized by the bump, become depleted by ionizing collisions and raise the temperature of the bulk plasma as pressure is increased.

characteristic. This observation validates earlier arguments [15] that such compensated probes were unreliable under exactly the circumstances predicted.

4. Measurements

With testing completed, the analyser was then used to measure the characteristics of antenna-driven plasmas. A wideband digital oscilloscope was synchronized to record the maximum and minimum of the current, corresponding to the most negative and most positive phases of the oscillating plasma potential, 180° apart. Positioned at the midpoint of the chamber was a Nagoya Type III antenna, 20 cm in length, driven by a 13.56 MHz variable-output generator capable of supplying $P_{rf} = 1.8$ kW. The plasma density was set in the range 10^{12-13} cm^{-3}. These parameters are similar to those in previous experiments in which accelerated electrons were reported [4–9] and also fell below the expected breakeven density at which collisional damping overtakes maximal Landau damping, calculated by Chen [1] to be n (cm^{-3}) = $1.63 \times 10^{12} f$ (MHz), which at $f = 13.56$ MHz is about 2×10^{13} cm^{-3}. The discharge has the bright blue colour typical of helicons in the W mode [16], and is the same discharge in which helicon waves have been studied with magnetic probes in other experiments.

Each data point was averaged over several plasma pulses using LabVIEW® software. The entire characteristic was typically 500 points and required about 1 h to produce and record. The data curves were smoothed by least-squares fitting consecutive intervals of the I–V characteristic to a third-order polynomial. Each interval contained 11 data points, which was found by trial and error to be an optimum number. By shifting the interval one data point at a time, the numerical noise is reduced sufficiently so that meaningful curves of the first derivative are obtained. Figure 14(a) shows an example of the analyser characteristic at the two opposite phases in the RF cycle. Also shown in comparison is the characteristic from a compensated Langmuir probe. All three curves indicate exponential dependence over three decades of signal level, indicative of a Maxwellian distribution with T_e between 3

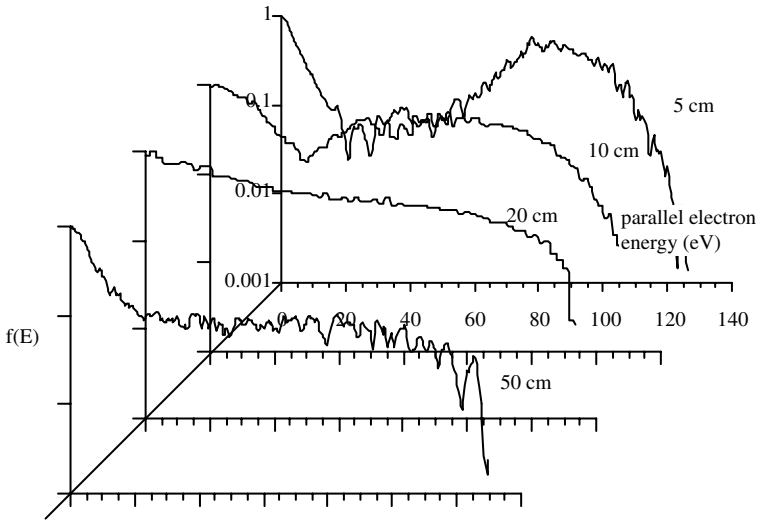

Figure 10. Evolution of the beam–plasma distribution function with increasing distance from the electron gun at a neutral gas pressure of 5 mTorr. The increasing distance thermalizes the beam faster than the increasing pressure, and after 20 cm the distribution function has gone from double-humped to monotonically decreasing.

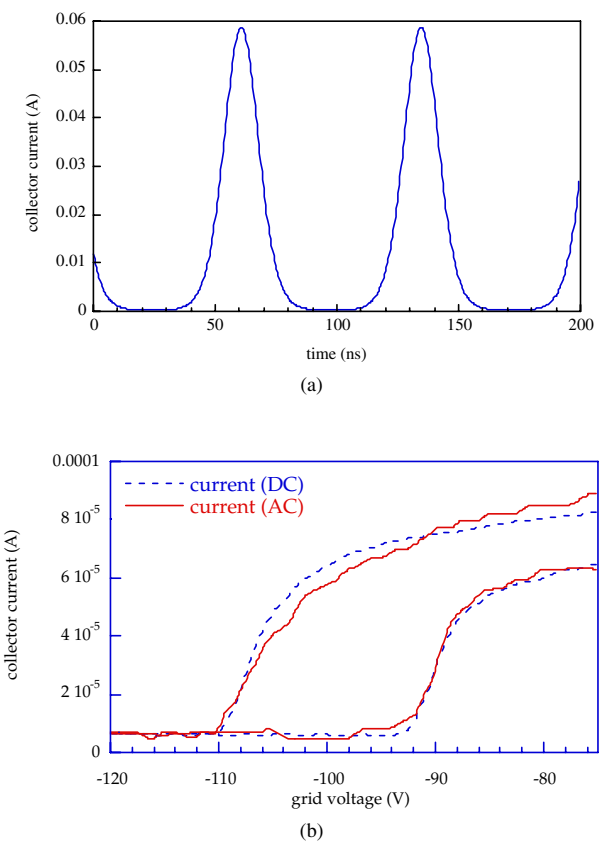

Figure 11. (a) Instantaneous current to the energy analyser due to fluctuations in plasma potential and density in a gun-produced plasma with the anode modulated. (b) Reconstructed analyser I–V curves of the RF-modulated electron beam in vacuum for two phases of the RF 180° apart (full curves), compared to the curves (dashed curves) for dc beams with a corresponding voltage difference.

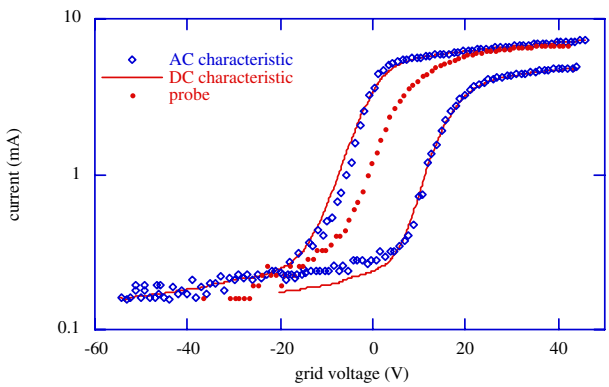

Figure 12. Reconstructed I–V curves taken by the energy analyser of the electron-gun-produced plasma with the anode modulated, as compared with the dc characteristics. The centre curve is the non-reconstructed, time-averaged curve obtained from an rf-compensated Langmuir probe.

and 3.5 eV. The first derivatives shown in figure 14(b) also indicate a good exponential fit over three decades. There is a slight difference (<20%) in the temperature that is obtained from these curves, which is within the statistical error found in previous measurements with Langmuir probes. The analyser could resolve current densities down to better than 0.1 mA cm^{-2}, while the total bulk electron current density under typical experimental conditions was several A cm^{-2}. This gives the energy resolution over more than three decades and was more than capable of detecting any non-Maxwellian beams which had been previously reported to have current densities greater than 10 mA cm^{-2} [4, 5].

Figure 15 shows the resulting curves of $f(v_\parallel)$ versus gas pressure at 360 G and the maximum RF power of 1800 W. The average parallel electron energy calculated from the average value of $E = 1/2mv_\parallel^2$ was unrealistically high, at around 5 eV. This is most likely due to two factors. First, due to its finite size the probe is not acting as an ideal planar probe, so that in fact a sampling of the perpendicular energies is included, since the probe sheath probably has a convex rather than planar shape. Second is the lack of digital bandwidth, or number of points sampled. Both of these effects produce a

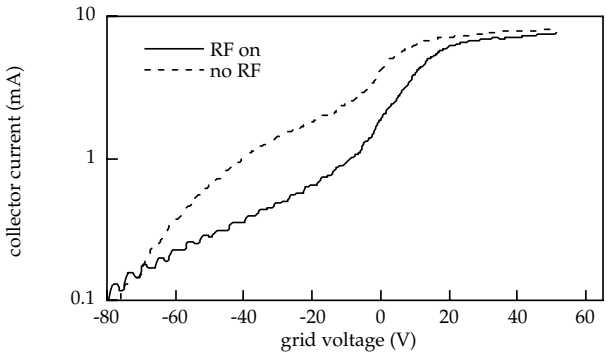

Figure 13. The characteristic from an RF-compensated Langmuir probe taken in a gun-produced plasma with a large percentage of fast electrons (dashed curve). Modulating the gun anode at 13.56 MHz causes the shape of the probe characteristic to change dramatically (full curve). The low-energy portions of the two curves show the same bulk temperature, but the RF modulation has decreased the population of high-energy electrons seen by the probe.

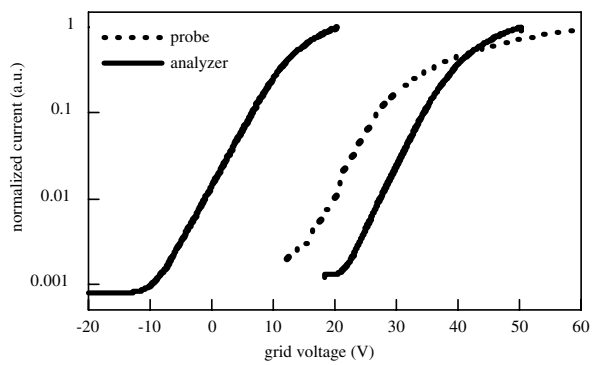

(a)

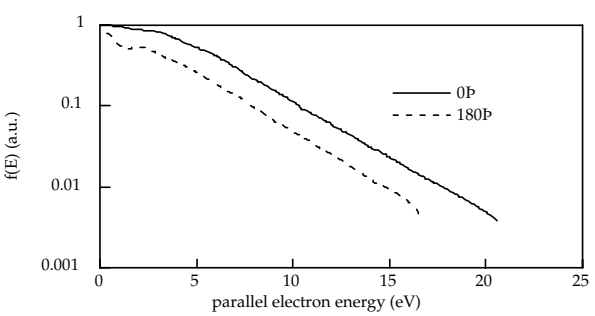

(b)

Figure 14. (a) I–V characteristics taken by the analyser (full curves) and a compensated Langmuir probe (dashed curve) in a helicon plasma at 2 mTorr Ar, 1 kW, 360 G, and 20 cm from the antenna. The analyser curves were reconstructed from signals at the maximum and minimum of the RF fluctuations, 180° apart in RF phase. (b) The first derivative of the analyser curves shown in (a), with the voltage axis shifted to represent electron energy. The slight separation of the curves is due to a small uncertainty in the plasma potential and is left in to make the curves visually distinguishable.

rounding effect of the characteristic near the plasma potential and subsequently one can underestimate of the number of low energy electrons in $f(v_\parallel)$. For our purposes this is an unimportant point, since the high-energy regions of the curves are where our attention is focused; and it is a feature of the distribution function in these regions, rather than the quantitative values of electron energy and density, with which we are concerned. Nevertheless, an electron temperature can be estimated from an exponential fit to the high-energy portion of $f(v_\parallel)$, and the variation of pressure over a decade causes a drop of only about 1 eV. More importantly, there is an absence of an abundance of fast electrons, in contrast to results in our beam-produced plasmas, where some deviation from a monotonically decreasing function was seen in $f(v_\parallel)$ even at high pressures and large distances from the gun.

The next logical parameter to change was magnetic field strength, since according to theory [1] and previous experiments [16–18] this has a dramatic effect on the wave propagation and, consequently, on the distribution function due to wave coupling. Figure 16 shows the results of varying the magnetic field over four values. There is a decided drop in electron energy in going from the unmagnetized plasma to the helicon plasma, which is due to the fact that there is a large increase in plasma density and hence collision rate. However, again none of the curves exhibit any pronounced deviation from monotonically decreasing, quasi-Maxwellian distribution functions.

It is apparent from these sets of curves that we were not observing any significant number of fast electrons. This negative result has the following physical implication. With the detection limit of the analyser at approximately 10^{-3} times the thermal electron current, in a 3 eV Maxwellian plasma any hot electrons not seen would have to have energy such that they satisfy the inequality $E^{1/2}\exp(-E/KT_e) < 10^{-3}$. This has a solution of $E \geqslant 25$ eV; electrons with this energy would only comprise approximately 0.02% of the distribution function. Higher energy electrons would have to have even lower density in order to escape detection; in fact, the most that there could possibly be to remain undetected at any particular energy would be $1.2 \times 10^{-3}\sqrt{E}$ with E being the electron energy. Let us say that we have the maximum number of such fast electrons all the way out to some unrealistic value such as, say, 200 eV. The entire integrated contribution of all of these electrons would increase the ionization rate by only a little more than 10% over a simple Maxwellian distribution. Clearly, any Landau-accelerated, wave-trapped, or other high-energy electrons make a negligible contribution to the ionization rate.

5. Conclusions

The principal difference between this and prior work is that the diagnostic used was experimentally demonstrated to function reliably under conditions similar to the helicon discharge. Although some authors do present convincing arguments as to why their probes are trustworthy, there has been little if any empirical data to support these claims. This is largely due to the limited amount of control the experimentalist has over the discharge parameters, so that it is at least extremely difficult to assess empirically the performance of the probes and the effects of RF fields on them, i.e. there is no null test available since large RF fields are always present. By constructing an electron gun with a modulated anode, we were able to bypass this problem, test, and debug the analyser under controlled conditions. To the best of our knowledge, this procedure has

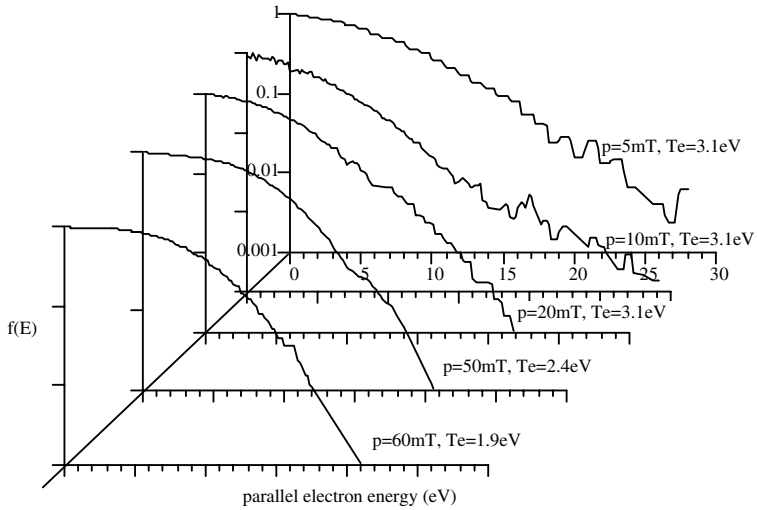

Figure 15. The first derivative of the analyser I–V characteristic versus pressure in a helicon plasma at 1800 W and 360 G magnetic field, 20 cm downstream from the antenna. In the higher energy thermal region ($E > 5$ eV), we can calculate from the slope an electron temperature in the range 2–3 eV as the pressure is dropped from 60 to 5 mTorr.

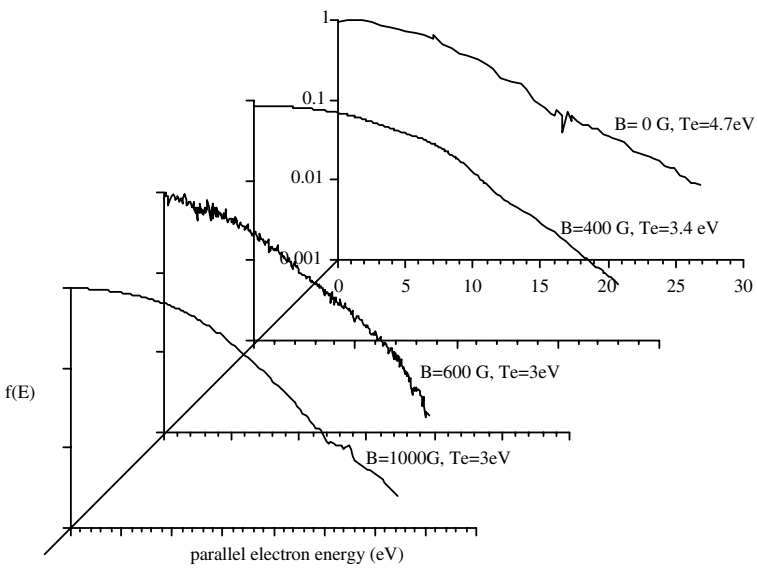

Figure 16. The first derivative of the analyser I–V characteristic versus magnetic field strength in a helicon plasma at 1800 W and 2 mTorr Ar pressure, 20 cm downstream from the antenna. As previously observed [19], the electron temperature inferred from the characteristic at $B = 0$ gives a higher temperature, probably caused by the lower density and collision rate.

not been carried out with any probe diagnostic in RF plasmas to date.

The second point of these measurements is that for the first time the characteristic of a helicon plasma has been measured completely free of any possible distortion from RF effects, either through changes in the probe–sheath voltage drop or changes in the distribution function itself. The curves we were able to construct are frozen snapshots of the current–voltage characteristics, and from these the instantaneous distribution of $v_\parallel$, which Landau damping involves, could be calculated. We chose this method because it provides a more direct picture of the thermal properties of the plasma than can be made by integrating the high-energy tail only [7] or by observing the light emission [12].

Finally, using a new diagnostic and data acquisition method, we found that our results disagreed with all previous experiments where fast electron beams *were* observed. Our measurements with the energy analyser described in this paper do not confirm the observations of previous experiments, nor do they lend credence to the notion of large populations of hot, non-Maxwellian electrons being present in the helicon discharge. There was also good agreement with the analyser data and that obtained using RF compensated Langmuir probes, which is not surprising, considering that no significant change was observed in the analyser characteristic at opposite phases of the RF cycle. Given the current resolution capabilities of the analyser, any such hyperthermal electron beam would comprise at most 2.4×10^{-4} times the bulk electron population in our discharge. Yet on the macroscopic level in terms of power efficiency, there is negligible difference between this source and others where such beams have been reported and attributed to being the fundamental mechanism

for such efficiency. It should be noted that the high-power, high-density plasma regime we are working in is not the same as all other experiments that have been previously done [5–9, 12], so it is a mistake to conclude that this work refutes previous experimental work. However, the high-density, high-efficiency helicon plasma was the motivation for the proposal of the Landau damping mechanism. In the light of our observations with the high-density plasma of this paper, the role of power absorption through Landau damping as the cause of high ionization efficiency and high density has been exaggerated.

References

[1] Chen F F 1991 *Plasma Phys. Control. Fusion* **33** 339
[2] Krall N A and Trivelpiece A W 1986 *Principles of Plasma Physics* (San Francisco Press) pp 520–32
[3] Fisch N J 1987 *Rev. Mod. Phys.* **59** 175
[4] Zhu P and Boswell R W 1991 *Phys. Fluids* B **3** 869
[5] Loewenhardt P K, Blackwell B D, Boswell R W, Conway G D and Hamberger S M 1991 *Phys. Rev. Lett.* **67** 2792
[6] Mieno T, Shoji T and Kadota K 1991 *Japan. J. Appl. Phys.* **31** 1879
[7] Molvik A W, Ellingboe A R and Rognlien T D 1997 *Phys. Rev. Lett.* **79** 233
[8] Molvik A W, Rognlien T D, Byers J A, Cohen R H, Ellingboe A R, Hooper E B, McLean H S, Stallard B W and Vitello P A 1996 *J. Vac. Sci. Technol.* A **14** 984
[9] Chen R T S and Hershkowitz N 1998 *Phys. Rev. Lett.* **80** 4677
[10] Hershkowitz N 1989 *Plasma Diagnostics* vol 1, ed O Auciello and D L Flamm (New York: Academic) ch 3
[11] Sudit I D and Chen F F 1994 *Plasma Sources Sci. Technol.* **3** 162
[12] Ellingboe A R, Boswell R W, Booth J P and Sadeghi N 1995 *Phys. Plasmas* **2** 1807
[13] Butler H S and Kino G S 1963 *Phys. Fluids* B **6** 1346
[14] Blackwell D D and Chen F F 1997 *Plasma Sources Sci. Technol.* **6** 569
[15] Chen F F 1997 *Plasma Phys. Control. Fusion* **39** 1533
[16] Ellingboe A R and Boswell R W 1996 *Phys. Plasmas* **3** 2797
[17] Chen F F and Chevalier G 1993 *J. Vac. Sci. Technol.* A **10** 1389
[18] Komori A, Shoji T, Miyamoto K, Kawai J and Kawai Y 1991 *Phys. Fluids* B **3** 893
[19] Blackwell D D 1994 *MS Thesis* University of California, Los Angeles
[20] Chen F F and Blackwell D D 1999 *Phys. Rev. Lett.* **82** 2677
[21] Conway G D, Perry A J and Boswell R W 1998 *Plasma Sources Sci. Technol.* **7** 337